Proceedings of the Combustion Institute, Volume 28, 2000/pp. 1933–1939

THE DEPENDENCE OF CHEMISTRY ON THE INLET EQUIVALENCE RATIO IN VORTEX-FLAME INTERACTIONS

JOHN B. BELL,[1] NANCY J. BROWN,[1] MARCUS S. DAY,[1] MICHAEL FRENKLACH,[1,2] JOSEPH F. GRCAR[3] AND SHAHEEN R. TONSE[1]

[1] *Lawrence Berkeley National Laboratory*
Berkeley, CA 94720, USA
[2] *Mechanical Engineering Department*
University of California at Berkeley
Berkeley, CA 94720, USA
[3] *Sandia National Laboratories*
Livermore, CA 94551, USA

The interaction of a vortex pair with a premixed flame serves as an important prototype for premixed turbulent combustion. In this study, we investigate the interaction of a counter-rotating vortex pair with an initially flat premixed methane flame. We compare computational solutions obtained using a time-dependent, two-dimensional adaptive low Mach number combustion algorithm that incorporates GRI-Mech 1.2 for the chemistry, thermodynamics, and transport of the chemical species. We discuss the mechanical nature of the flame-vortex interaction and the features of the interaction that are strongly affected by fuel equivalence ratio, ϕ. We find that the circulation around the vortex scours gas from the preheat zone in front of the flame, making the interaction sensitive to equivalence ratio. For cases with $\phi \approx 1$, the peak mole fraction of CH across the flame is relatively insensitive to the vortex, whereas for richer flames we observe a substantial and rapid decline in the peak CH mole fraction, commencing early in the flame-vortex interaction. The peak concentration of HCO is found to correlate, in both space and time, with the peak heat release across a broad range of equivalence ratios. The model also predicts a measurable increase in C_2H_2 as a result of interaction with the vortex and a marked increase in the low-temperature chemistry activity.

Introduction

Turbulence affects the process of methane combustion through a wide variety of mechanisms. Traditional approaches, based on asymptotic analysis, show that velocity-induced tangential strain at the flame surface can dramatically enhance or suppress combustion activity in the flame zone depending on Lewis number. These effects have been studied using results from steady flat-flame counterflow experiments (see Refs. [1–5]). As discussed in the review by Peters [6], this type of information can be readily incorporated into engineering models through the flamelet concept.

Research aimed at understanding transient effects in turbulent flows has led investigators to study the interaction of a single vortical structure with a premixed flame. These flows offer advantages of being more repeatable and more amenable to analysis and experimental diagnostics than fully developed turbulent flow. Such studies typically consider either a planar vortex pair (e.g., see Refs. [7–11]) or an axisymmetric toroidal vortex (e.g., see Refs. [12–19]). Vortex-driven flame quenching has been studied computationally using both single-step [20] and two-step [21] reaction mechanisms. The performance of certain flame markers in the presence of time-dependent vortical perturbations has been assessed in simulations using skeletal C_1 methane chemistry [7,22] and more complete description of C_1 and C_2 chemistry [23]. Hilka et al. [24] assess the ability of a 4-step mechanism to predict combustion heat release in this configuration, using a more detailed 52-step mechanism as a baseline.

While most of the experimental data on methane flame quenching and combustion markers focus on lean flames, Nguyen and Paul [8] considered a rich methane flame. Their results are particularly interesting for several reasons. First, they predict dramatic changes in species concentrations, notably CH and OH, that are not predicted by counterflow flame simulations [2]. This suggests that a flamelet model based solely on flat-flame data may be inadequate for transient flow field interactions. Second, the limited number of computational studies available for modeling rich, multidimensional vortex-flame interactions yield results that are somewhat inconsistent with the experiment. For example, Najm et al. [23] computed a flow problem similar to the Nguyen and Paul experiment. They used the GRI-Mech 1.2 [25] reaction mechanism and a smaller, faster vortex with less nitrogen dilution; however, their simulations

Report Documentation Page

Form Approved
OMB No. 0704-0188

1. REPORT DATE	2. REPORT TYPE	3. DATES COVERED
04 AUG 2000	**N/A**	**-**

4. TITLE AND SUBTITLE	5a. CONTRACT NUMBER
The Dependence of Chemistry on the Inlet Equivalence Ratio in Vortex-Flame Interactions	5b. GRANT NUMBER
	5c. PROGRAM ELEMENT NUMBER
6. AUTHOR(S)	5d. PROJECT NUMBER
	5e. TASK NUMBER
	5f. WORK UNIT NUMBER
7. PERFORMING ORGANIZATION NAME(S) AND ADDRESS(ES) **Lawrence Berkeley National Laboratory Berkeley, CA 94720, USA**	8. PERFORMING ORGANIZATION REPORT NUMBER
9. SPONSORING/MONITORING AGENCY NAME(S) AND ADDRESS(ES)	10. SPONSOR/MONITOR'S ACRONYM(S)
	11. SPONSOR/MONITOR'S REPORT NUMBER(S)

12. DISTRIBUTION/AVAILABILITY STATEMENT
Approved for public release, distribution unlimited

13. SUPPLEMENTARY NOTES
See also ADM001790, Proceedings of the Combustion Institute, Volume 28. Held in Edinburgh, Scotland on 30 July-4 August 2000., The original document contains color images.

14. ABSTRACT

15. SUBJECT TERMS

16. SECURITY CLASSIFICATION OF:			17. LIMITATION OF ABSTRACT	18. NUMBER OF PAGES	19a. NAME OF RESPONSIBLE PERSON
a. REPORT	b. ABSTRACT	c. THIS PAGE			
unclassified	**unclassified**	**unclassified**	**UU**	**7**	

Standard Form 298 (Rev. 8-98)
Prescribed by ANSI Std Z39-18

failed to reproduce several key features observed in the experiment.

In this paper, we study in detail the interaction of a vortex with premixed N_2-diluted methane flames that have equivalence ratios in the range $\phi = 0.76$–1.28. The vortex we impose matches the strength, core separation, and speed of that observed in the Nguyen and Paul experiment. Although our configuration is close to the actual experimental conditions, our initial premixed flame is flat and oriented normal to the inlet flow. The simulations therefore lack a small lateral velocity component associated with the V-flame configuration of the related experiment. We carry out these studies by numerical simulation using a parallel, adaptive low Mach number combustion algorithm developed by Day and Bell [26]. All of the computations use chemistry, transport, and thermodynamic databases specified in GRI-Mech 1.2. Our results match the CH behavior reported in Nguyen and Paul's experiment. In addition, we observe that the flame's response to the vortex is a strong function of the inlet flow equivalence ratio. We find that mole fraction of HCO correlates, in both position and time, with the heat release of the methane flame. Finally, we find that in spite of the agreement in CH profiles, our simulations do not reproduce the experimentally observed behavior of OH.

Numerical Model

Our computational approach uses a hierarchical adaptive mesh refinement (AMR) algorithm based on an approximate projection formulation for integrating the momentum equations [27] and subsequently extended to low Mach number flows [28]. The projection algorithm is coupled to conservation equations for chemical species and enthalpy. The single-grid algorithm is implemented in a structured uniform grid setting and incorporated into an AMR framework that employs a recursive time-stepping procedure over refinement levels. We sketch the model and numerical implementation below; the reader is referred to Ref .[26] for details.

Our model is based on a conservative form of the low Mach number combustion model introduced by Rehm and Baum [29], subsequently derived from low Mach number asymptotic analysis by Majda and Sethian [30]. We consider a gaseous mixture, ignoring Soret and Dufour effects, body forces, and radiative heat transfer, and assume a mixture model for species diffusion [31,32]. For an unconfined domain, we have

$$\frac{\partial \rho U}{\partial t} + \nabla \cdot \rho UU = -\nabla \pi + \nabla \cdot \tau \qquad (1)$$

$$\frac{\partial \rho Y_m}{\partial t} + \nabla \cdot U \rho Y_m = \nabla \cdot \rho \mathcal{D}_m \nabla Y_m - \dot{\omega}_m \qquad (2)$$

$$\frac{\partial \rho h}{\partial t} + \nabla \cdot U \rho h = \nabla \cdot \frac{\lambda}{c_{\mathrm{p,mix}}} \nabla h + \sum_m \nabla \cdot h_m \left(\rho \mathcal{D}_m - \frac{\lambda}{c_{\mathrm{p,mix}}} \right) \nabla Y_m \qquad (3)$$

where ρ is the density, U is the velocity, π is the pressure variation from a uniform ambient pressure, Y_m is the mass fraction of species m, h is the mass-weighted enthalpy of the gas mixture, T is the temperature, and $\dot{\omega}_m$ is the net destruction rate for ρY_m due to chemical reactions. Also, λ is the thermal conductivity, τ is the stress tensor, $c_{\mathrm{p,mix}}$ is the specific heat of the mixture, and $h_m(T)$ and $\mathcal{D}_m$ are the enthalpy and species mixture-averaged diffusion coefficients of species m, respectively. These evolution equations are supplemented by an equation of state for a perfect gas mixture:

$$p_0 = \rho R_{\mathrm{mix}} T = \rho \mathcal{R} T \sum_m \frac{Y_m}{W_m} \qquad (4)$$

where W_m is the molecular weight of species m.

In the low Mach number limit, the thermodynamic pressure given by equation 4 remains approximately constant as the flow evolves. Differentiating the equation of state in the frame of the fluid, and using the conservation equations to replace advective derivatives, we obtain an elliptic constraint on the evolving velocity field:

$$\nabla \cdot U = \frac{1}{\rho c_{\mathrm{p}} T} \left(\nabla \cdot \lambda \nabla T + \sum_m \rho \mathcal{D}_m \nabla Y_m \cdot \nabla h_m \right) + \frac{1}{\rho} \sum_m \frac{W}{W_m} \nabla \cdot \rho \mathcal{D}_m \nabla Y_m + \frac{1}{\rho} \sum_m \left(\frac{h_m(T)}{c_{\mathrm{p,mix}} T} - \frac{W}{W_m} \right) \dot{\omega}_m \equiv S \qquad (5)$$

where

$$W = (\Sigma_m Y_m / W_m)^{-1}$$

and

$$c_{\mathrm{p,mix}} = \Sigma_m Y_m dh_m / dT$$

The single-grid scheme that forms the basis for our adaptive algorithm combines a symmetric operator-split coupling of chemistry and diffusion processes with a projection method for incorporating the velocity divergence constraint. First, equations 1–3 are advanced in time using a second-order Godunov scheme for convective terms and a time-centered Crank-Nicolson discretization for diffusion. Because the transport coefficients depend on both temperature and composition, we adopt a sequential, predictor-corrector scheme to guarantee second-order treatment of nonlinear diffusion effects.

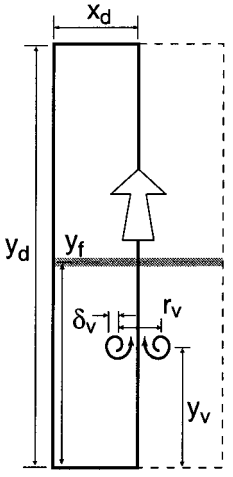

FIG. 1. Schematic of the premixed methane flame-vortex problem. The shaded line represents the position of the flame, and the swirl lines represent the initial vortex. We impose symmetry along the sides of the 0.8 × 4.0 cm domain to avoid modeling the dotted region.

The chemistry is advanced using time-implicit backward differentiation methods [33]. The implicit diffusion and chemistry components of the algorithm are time split symmetrically to ensure that the composite algorithm remains second order. The velocity field resulting from the advection/diffusion/chemistry step is then decomposed using a density-weighted approximate projection. Numerically, the projection step requires the solution of a variable-coefficient linear elliptic equation. The component satisfying the constraint, equation 5, updates the velocity field, and the remainder updates the perturbational pressure. The explicit procedure for the treatment of advection terms necessitates a Courant-Friedrichs-Lewy–type (CFL-type) time-step restriction. Since the advective time scale is typically larger than the fastest time scales associated with the chemical kinetics, this does not appear to be a serious disadvantage for time-dependent simulations.

We note that because of the fractional-step nature of the overall approach, it is impossible to satisfy the equation of state while conserving species and enthalpy discretely. We add a correction to equation 5:

$$\frac{f}{\gamma p_{\text{amb}}} \frac{\delta p}{\Delta t}$$

where $\delta p = p_0 - p_{\text{amb}}$, p_{amb} is the ambient pressure, Δt is the numerical time step, and γ is the ratio of specific heats. This forcing term prevents the algorithm from drifting an appreciable amount off the equation of state. The details of this correction and its effects are discussed in Ref. [26]; however, we note that in the calculations presented here the thermodynamic pressure deviates no more than 0.5% from the ambient atmospheric pressure.

The extension of the above algorithm to adaptive mesh refinement is based on a hierarchical refinement strategy. Our methodology uses a system of overlaid grids with successively finer spacing in time and space. Fine grids are formed by uniformly dividing coarse cells in each direction. Increasingly finer levels, each consisting of a union of rectangular grid patches, overlay coarser grid levels until the solution is adequately resolved. An error-estimation procedure identifies where refinement is needed, and grid-generation procedures dynamically create or remove rectangular fine grid patches as requirements change.

The complete adaptive algorithm has a number of desirable properties. The overall method is second-order accurate in space and time and discretely conserves species mass and enthalpy. Furthermore, the algorithm satisfies a free-stream preservation property such that non-reacting isothermal flow remains numerically isothermal during species transport. The methodology has been implemented for distributed memory parallel processors using the BoxLib class libraries described by Rendleman et al. [34].

Results

We conducted a detailed study of a counter-rotating pair of vortices interacting with N_2-diluted premixed methane-air flames. We focus the discussion on two aspects of the results. First, we are interested in characterizing the mechanical nature of the flame-vortex interaction. Second, we want to understand how this behavior affects the combustion process as a function of flame stoichiometry.

The computational study approximates the experimental conditions of Nguyen and Paul. Following Najm et al., we approximate the V-flame experiment as a flat premixed flame oriented normal to the inlet flow and superimpose a velocity field due to a periodic array of counter-rotating vortex pairs with Gaussian cores $\delta_v = 2.25$ mm wide and centers $r_v = 0.25$ cm apart. The vortex pair propagates upward with a self-induced velocity of 110 cm/s. These parameters produce a vortex pair with the same width and propagation speed as reported for the vortex pair in the Nguyen and Paul experiment. We numerically evolve only the left vortex, as indicated in Fig. 1. Our base computational domain is $x_d = 8$ mm wide and $y_d = 4$ cm high, with the boundary along the right side corresponding to the vortex centerline. The periodic configuration results from symmetry boundary conditions imposed on the sides of the domain. Reactants flow in at the bottom, and combustion products exit through the top.

We position the initial premixed flame so that the peak mole fraction of HCO occurs at $y_f = 2$ cm (see Fig. 1). Cell-centered values are initialized using cell averages of a refined PREMIX [35] solution. A vortex is superimposed on this flow field, centered halfway between the inlet and flame. We cover the entire domain with a uniform coarse mesh ($\Delta x = 250$ μm) and then place up to two refined grid levels,

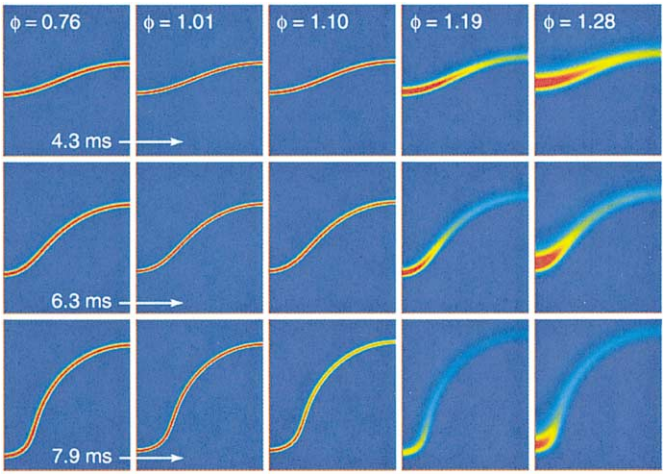

FIG. 2. CH mole fraction. In each column, the three frames correspond approximately to 4.3, 6.3, and 7.9 ms simulation time from the initial conditions (see Fig. 1). The color scale in each column is normalized to peak values of X_{CH} = (0.23, 7.76, 10.8, 3.66, 0.30) × 10^{-7}, respectively. The frames represent 8 × 9.5 mm subregions of the domain near the flame surface.

each with Δx decreased by a factor of 2, to resolve the flame zone. The resulting resolution is equivalent to that of a 128 × 640 uniform grid calculation with Δx = 62.5 μm. To determine whether image vortices introduced by the symmetry boundary conditions significantly impact these results, we also performed calculations on larger domains. Results on the smaller domain depicted in Fig. 1 are insensitive to the domain size for the first 10 ms of simulation time; for longer times there are noticeable edge effects. Where we report longer time results, we use data computed on domains sufficiently large that the edge effects are not manifest.

The inlet fuel for the simulations consisted of methane uniformly mixed with nitrogen-diluted air (N_2:O_2 = 6.28:1, by volume). Five stoichiometries were considered: ϕ equal to 0.76, 1.01, 1.10, 1.19, and 1.28. In Fig. 2, we present snapshots depicting the mole fraction of CH for each stoichiometry. At 7.9 ms, the vortex center has traveled 80% of the distance initially separating the flame and vortex and has interacted with the flame significantly. The extent of the simulated decline in the CH signal is dependent on the overall flame stoichiometry. There is no noticeable change in the peak value of CH along the flame surface for ϕ = 0.76 and only a very small decline for the ϕ = 1.01 case. However, at ϕ = 1.10, the decline becomes pronounced, and it steepens with further increases in the equivalence ratio.

The case ϕ = 1.19 corresponds to the stoichiometry (and nitrogen dilution) used in Nguyen and Paul's experiment. They observe a two- to threefold decrease in the averaged CH signal before it abruptly disappears. The loss of signal occurs throughout the flame sheet wrapped around the vortex and occurs about 7 ms after the vortices first begin to distort the flame. Examination of our numerical results indicates that CH concentration for this case exhibits a similar rapid decline, leading eventually to a nearly 10-fold decrease. This simulated rate of decrease is consistent with the planar laser-induced fluorescence signal descending to its noise level in the time interval observed. Moreover, Fig. 2 shows that the simulated CH concentration declines precisely in the region identified by Nguyen and Paul.

A more detailed examination of the computational results indicates that there is actually a qualitative shift in the behavior of CH between ϕ = 1.10 and ϕ = 1.19. In Fig. 3 we show time histories of the peak molar concentration of each species along the right boundary of the computational domain for the two cases. In the rich cases ($\phi \geq 1.19$), the peak in CH declines more rapidly than the peak heat release; the opposite is true in the lean cases ($\phi \leq$ 1.10).

In this region, strain effects induced by the flow field components tangential to the flame surface associated with the impinging vortex result in a strong, positive flame stretch. Flame curvature caused by flow components normal to the flame surface result in a much weaker negative stretch. The strain and net stretch are at a maximum along the centerline (the right boundary of the computational domain) and locally decrease as we move along the flame surface. Classical planar strained flame analysis (cf. Ref. [36], and for complex chemistry, see Kee et al. [37]) predicts a reduction in temperature and a steepening of gradients with increasing strain but does not predict a change in flame structure. The experiments and our computations corroborate the first two effects but also show that the interaction clearly modifies the flame structure.

We note that, unlike the stretched steady flat-flame case, the strong circulation pattern around the vortex leads to strong and variable tangential flow along the flame front. As a part of this process the

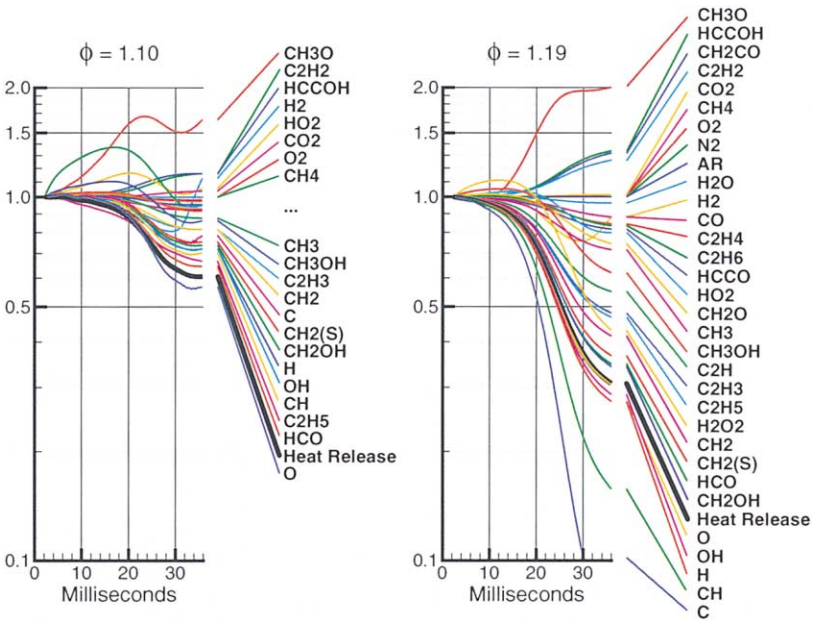

FIG. 3. Time history of the peak values of molar concentration, normalized to their respective values at $t = 2$ ms. Normalization is made at this later time to avoid initial transients as the PREMIX solution adjusts to the AMR grid. Note that these data are taken from simulations on very large 1.2×5.6 cm domains to avoid edge effects at later times in the flame-vortex interaction.

circulation of the vortex entrains material from the preheat region in front of the flame, replacing the equilibrium distribution of combustion intermediates upstream of the primary heat-release zone with the inlet mixture. We refer to this specific mechanical process as one that "scours" combustion intermediates from the front of the flame. The net effect of this process depends on the composition of the fluid in front of the flame, which in turn depends on the equivalence ratio.

To isolate the role that this vortex-induced scouring has on flame chemistry, we have modeled the process in one dimension with source terms that replace material in the preheat region in front of the flame with the inlet mixture. This one-dimensional model thus represents the chemical effects of scouring without the fluid mechanical effects of strain. Numerical tests with this one-dimensional model indeed show that for the richer flame, $\phi = 1.19$, the scouring effect disrupts the chemical pathways, leading to the production of CH. Conversely, we observed essentially no change for the lean $\phi = 1.10$ case. These results match the behavior of our two-dimensional study.

Although the notion of vortex scouring in combination with effects due to stretch and strain describe the mechanisms by which the vortex modulates the flame, the net result of this modification can be quite complex. It is compelling to conjecture that the dominant effect in the rich case is the removal of H_2 from the front of the flame, since H_2 profiles in the unperturbed flame extend well into the region most affected by the impinging vortex. However, tests of this hypothesis with the one-dimensional scouring model described above show that this is not the case. In general, the effects of vortex scouring depend on preferential diffusion effects in competition with reactions and on the specific reaction pathways that are dominant in a given region of the flame.

The flame structures were also analyzed using reaction path analysis. The reaction pathways are those that one would expect—namely, the C_1 pathway to formyl radical and an enhancement of the C_2 pathways with increasing equivalence ratio. The sensitivity analysis showed the dominance of reactions that are most important in controlling the size of the radical pool, and in many cases the sensitivities showed self-similarity, indicating that only a few variables control the state of the system. In agreement with Najm et al., we find that the formyl radical, HCO, is a reliable marker for heat release. The numerical results presented in Fig. 3 and similar analyses for other stoichiometries confirm this for flames interacting with vortices. The dramatic decrease of CH in rich flames is linked to the decrease of H atom concentrations and triplet methylene and decreases in important production rates. Interestingly, some

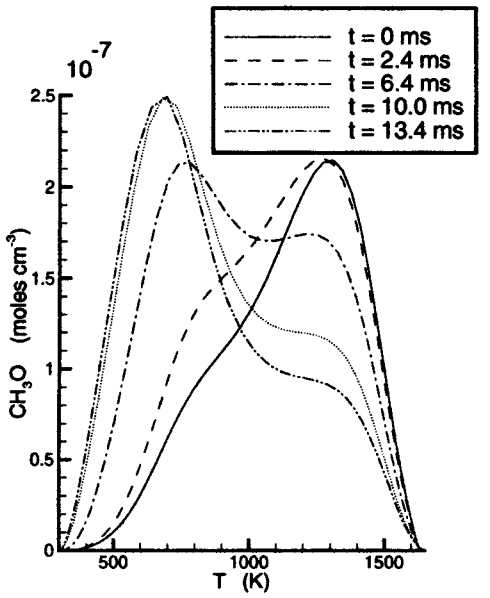

FIG. 4. CH_3O profiles along the vortex centerline for $\phi = 1.19$. During the flame-vortex interaction, there is a marked enhancement of CH_3O concentration in low-temperature regions.

species increase in concentration in low-temperature zones. For example, for $\phi = 1.19$, the species CH_3O, C_2H_2, HO_2, CH_3, HCCOH, CH_2CO, and CO_2 increase. The most dramatic example occurs for CH_3O, as shown in Fig. 4. We note a shift of the peak concentration to lower temperatures as the vortex couples more strongly with the flame. Sensitivity analysis indicates a linkage between the increase in CH_3O and the decline in CH. Another noteworthy feature is the increase in the C_2H_2 concentration, which occurs as a result of the flame-vortex interactions. This prediction is potentially significant for soot production.

Conclusions

Numerical simulations of vortex-flame interactions have revealed a strong dependence of CH behavior on equivalence ratio. Analysis of this behavior has shown that the vortex not only stretches and strains the flame but also scours material from the preheat region in front of the flame and at early times replaces it with inlet gases. This scouring effect produces the dramatic decline in CH observed experimentally by Nguyen and Paul. The model predicts a measurable increase in C_2H_2 as a result of the vortex and a marked increase in the low-temperature chemistry activity.

The model fails to reproduce the enhancement of OH observed by Nguyen and Paul. One possibility is that, with our current limited knowledge of the low-temperature chemistry, some unknown chemistry or imprecise knowledge of thermochemistry might lead to the experimentally observed rise in OH signal. The approximation of the V-flame configuration using a flat flame and enhanced mixing not represented in the two-dimensional flow model are other possible sources of discrepancy.

Acknowledgments

The work of JB and MD was supported by the Applied Mathematics Program of the U.S. Department of Energy Office of Mathematics, Information, and Computational Sciences and that of NB, MF, and ST by the Laboratory Directed Research and Development Program of Lawrence Berkeley National Laboratory under the U.S. Department of Energy under contract no. DE-AC03-76SF00098. The work of JG was supported by Sandia National Laboratories, a multiprogram laboratory operated by Sandia Corporation, a Lockheed Martin Company, for the U.S. Department of Energy under contract no. DE-AC04-94AL85000.

REFERENCES

1. Egolfopoulos, F., *Proc. Combust. Inst.* 25:1365–1373 (1994).
2. Kee, R. J., Miller, J. A., Evans, G. H., and Dixon-Lewis, G., *Proc. Combust. Inst.* 22:1479–1494 (1988).
3. Law, C. K., *Proc. Combust. Inst.* 22:1381–1402 (1988).
4. Petrov, C., and Ghoniem, A., *Combust. Flame* 102:401–417 (1995).
5. Rogg, B., *Combust. Flame* 73:45–46 (1988).
6. Peters, N., *Proc. Combust. Inst.* 21:1231–1250 (1986).
7. Najm, H. N., Paul, P. P., Mueller, C. J., and Wyckoff, P. S., *Combust. Flame* 113:312–332 (1998).
8. Nguyen, Q.-V., and Paul, P. H., *Proc. Combust. Inst.* 26:357–364 (1996).
9. Paul, P. H., and Najm, H. N., *Proc. Combust. Inst.* 27:43–50 (1998).
10. Samaniego, J.-M., *1993 Annual Research Briefs*, Center for Turbulence Research, Stanford University, Stanford, CA, p. 205–218.
11. Samaniego, J.-M., and Mantel, T., *Combust. Flame* 118:537–556 (1999).
12. Driscoll, J. F., Sutkus, D. J., Roberts, W. L., Post, M. E., and Goss, L. P., *Combust. Sci. Technol.* 96:213 (1994).
13. Mueller, C. J., Driscoll, J. F., Reuss, D. L., and Drake, M. C., *Proc. Combust. Inst.* 26:347–355 (1996).
14. Mueller, C. J., Driscoll, J. F., Reuss, D. L., Drake, M. C., and Rosalik, M. E., *Combust. Flame* 112(3):342–358 (1998).
15. Mueller, C. J., Driscoll, J. F., Sutkus, D. J., Roberts, W. L., Drake, M. C., and Smooke, M. D., *Combust. Flame* 100:323–331 (1995).
16. Roberts, W. L., and Driscoll, J. F., *Combust. Flame* 87:245 (1991).

17. Roberts, W. L., Driscoll, J. F., Drake, M. C., and Goss, L. P., *Combust. Flame* 98:58–69 (1993).
18. Roberts, W. L., Driscoll, J. F., Drake, M. C., and Ratcliffe, J. W., *Proc. Combust. Inst.* 24:169 (1992).
19. Rolon, J. C., Aguerre, F., and Candel, S., *Combust. Flame* 100:422–429 (1995).
20. Poinsot, T. J., Veynante, D., and Candel, S. M., *J. Fluid Mech.* 228:561–606 (1991).
21. Mantel, T., *1994 Annual Research Briefs,* Center for Turbulence Research, Stanford University, Stanford, CA, pp. 45–76.
22. Najm, H. N., and Wyckoff, P. S., *Combust. Flame* 110:92–112 (1997).
23. Najm, H. N., Knio, O. M., Paul, P. P., and Wyckoff, P. S., *Combust. Sci. Technol.* 140:369–403 (1998).
24. Hilka, M., Veynante, D., Baum, M., and Poinsot, T. J., *10th Symposium on Turbulent Shear Flows,* 2 (19):19–24 (1995).
25. Frenklach, M., Wang, H., Goldenberg, M., Smith, G. P., Golden, D. M., Bowman, C. T., Hanson, R. K., Gardiner, W. C., and Lissianski, V., *GRI-Mech—An Optimized Detailed Chemical Reaction Mechanism for Methane Combustion,* Gas Research Institute report GRI-95/0058; see also http://www.me.berkeley.edu/gri_mech/.
26. Day, M. S., and Bell, J. B., *Combust. Theory Model,* in press (2000).
27. Almgren, A. S., Bell, J. B., Colella, P., Howell, L. H., and Welcome, M., *J. Comput. Phys.* 142:1–46 (1998).
28. Pember, R. B., Howell, L. H., Bell, J. B., Colella, P., Crutchfield, W. Y., Fiveland, W. A., and Jessee, J. P., *Combust. Sci. Technol.* 140:123–168 (1998).
29. Rehm, R. G., and Baum, H. R., *NBSJ Res.* 83:297–308 (1978).
30. Majda, A., and Sethian, J. A., *Combust. Sci. Technol.* 42:185–205 (1985).
31. Kee, R. J., Dixon-Lewis, G., Warnatz, J., Coltrin, M. E., and Miller, J. A., Sandia report SAND86-8246.
32. Warnatz, J., in *Numerical Methods in Flame Propagation* (N. Peters, and J. Warnatz, eds.), Friedrich Vierweg and Sohn, Wiesbaden, Germany, 1982.
33. Brown, P. N., Byrne, G. D., and Hindmarsh, A. C., *SIAM J. Sci. Stat. Comput.* 10:1038–1051 (1989).
34. Rendleman, C. A., Beckner, V. E., Lijewski, M., Crutchfield, W. Y., and Bell, J. B., *Computing and Visualization in Science,* Lawrence Berkeley National Lab report LBNL-43154.
35. Kee, R. J., Grcar, J. F., Smooke, M. D., and Miller, J. A., Sandia report SAND85-8240.
36. Williams, F. A., *Combustion Theory, 2nd ed.,* Addison-Wesley, New York, 1985, p. 418.
37. Kee, R. J., Miller, J. A., and Evans, G. H., *Proc. Combust. Inst.* 22:1479–1494 (1988).